

A Multi-Scale Homogenization Technique Applied to the Elastic Properties of Solders

A. Brandmair, W. Müller, M. Savenkova, S. Sheshenin

In modern microelectronic systems solder materials are frequently used. Consequently, it is of great importance to predict their lifetime and stability. In order to perform such an analysis, material properties are required. Since electronic devices and therefore the amounts of used materials become smaller and smaller, the influence of a changing microstructure on the mechanical properties must be examined. First, some analytical methods will be presented leading to upper and lower bounds for standard solder alloys. They also allow for an examination of the influence of certain micro-geometries. Second, a multi-scale approach is used in order to perform a more general analysis of different micro-structures. The constitutive equations are stated and a homogenization technique for elastic properties of arbitrary structures is derived. The resulting equations are solved numerically and the results are presented. For lamellar-type of structures, closed-form formulas are derived and the results will be compared to the numerical ones.

1 Introduction

In microelectronic applications solder alloys fulfill an important role. On the one hand side they guarantee the mechanical connection between, *e.g.*, the chip and a printed circuit board. On the other hand side they also establish electrical contact between the components. Therefore the stability of the applied solder-materials is of particular interest for the lifetime-prediction of microelectronic devices. All of the solder alloys that are used show some kind of micro-structural change during aging. For example, the microstructure of an eutectic AgCu28-solder changes over time due to phase-separation followed by coarsening. This is shown in Figure 1.

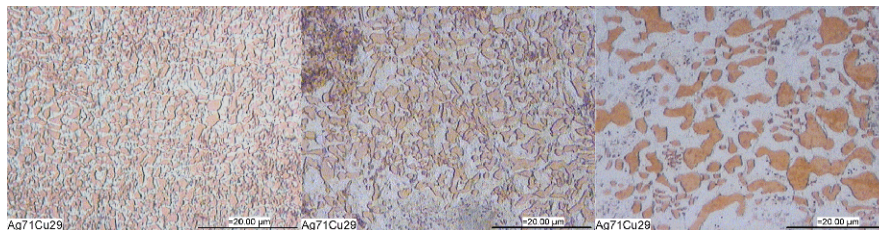


Figure 1. Coarsening of an AgCu28 structure after 2h, 20h and 40h

The development of this particular microstructure is based on the tendency of the solder system to minimize its internal surface. It can be described by using an extended diffusion equation and has been examined in-depth in [1]. As the amount of used solder-material is in general very small, changes in the microstructure cannot be neglected when predicting the reliability of such structures. Due to this reason it is important to take the different length-scales into account. In particular it is of interest to examine how the changing microstructure influences the macroscopic material-properties. A direct calculation, *e.g.*, by FE-simulations, is based on rather complex FE-meshes and time-consuming. For this reason a method by means of which reliable results for the material properties can be obtained without having to model the exact structure seems rather useful. In this context, the procedure of homogenizing material properties has shown to be quite promising. The obtained homogenized, effective properties should be able to reproduce the real behaviour of the material to a great extent and would enable us to perform continuum-based FE-simulations of microelectronic devices in order to predict their lifetime and stability without a detailed discretization of the complete micro-structure.

2 Boundary Estimates for the Mechanical Properties of Selected Solder-Materials

For the examination of boundaries for the mechanical properties of solder-materials two binary solders, namely silver-copper (AgCu), tin-lead (SnPb) and tin-silver (SnAg), were chosen. Furthermore only elastic properties will be investigated and analyzed by means of homogenization. We start by deriving YOUNG's modulus from the values of the polycrystalline stiffness-tensor C_{ijkl} for copper. This serves as an example in order to validate results for the elastic constants which were obtained by using the Embedded-Atom-Method (EAM), which in turn is based on inter-atomic potentials [2]. Figure 2a shows the results for the stiffness-tensor of a single crystal made of copper. The values in brackets show results obtained from the literature for comparison. Based on these values, a direction-dependent compliance S'_{11} has been calculated by using the following formula where S is the inverse of the stiffness-tensor [3]. Note that this formula only holds for cubic crystal symmetry:

$$S'_{11} = S_{11} - 2(S_{11} - S_{12} - \frac{1}{2}S_{44}) \left[\frac{(\sin(\nu) \cos(\varphi))^2 (\sin(\nu) \sin(\varphi))^2 + (\sin(\nu) \sin(\varphi))^2 \cos(\nu)^2 + (\sin(\nu) \cos(\varphi))^2 \cos(\nu)^2}{+ (\sin(\nu) \cos(\varphi))^2 \cos(\nu)^2} \right]. \quad (1)$$

The angles ν and φ in (1) are the inclination and the azimuth of a respective spherical coordinate system. In Figure 2b S'_{11} , the first entry of the direction-dependent compliance tensor, is plotted. $x_1 - x_3$ in Figure 2b are the main crystallographic axes of the cubic copper. In Figure 2c the results for YOUNG's modulus via averaging over the unit sphere are presented. Young's modulus was calculated forming the reciprocal of the mean value of S'_{11} .

This transformation of anisotropic material-parameters has been used to validate the elastic-isotropic parameters, used for homogenization.

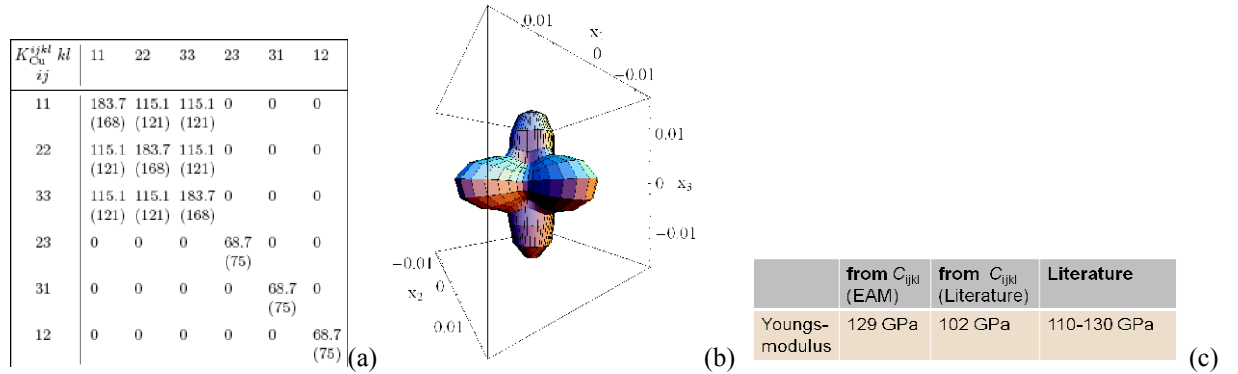


Figure 2. (a) Stiffness-tensor for copper via EAM (values from literature in brackets), (b) Direction-dependence of the compliance-tensor of copper, (c) YOUNG's modulus for copper

The parameters shown in Table 1 were then used in order to obtain first estimates for the bulk modulus k and for the shear modulus μ of the alloys that were just mentioned. Intuitively speaking, the different phases are connected in parallel or in series, and these leads to lower and upper bounds, respectively, which are also known as VOIGT and REUSS limits. The exact geometric form of the "inclusions," and therefore the exact form of the microstructure of the alloy, is not taken into account this way and just the volume fractions, c_i , need to be known:

$$\frac{1}{\sum_{i=1}^N c_i / k_i} \leq k \leq \sum_{i=1}^N c_i k_i, \quad \frac{1}{\sum_{i=1}^N c_i / \mu_i} \leq \mu \leq \sum_{i=1}^N c_i \mu_i. \quad (2)$$

type of metal	YOUNG's modulus (polycrystal)	YOUNG's modulus from C_{ijkl} (averaged over unit sphere)	Poisson's ratio, ν	shear modulus, μ , predicted	bulk modulus, k , predicted
Silver Ag	83 GPa	81/65 GPa	0,37	30 GPa	106 GPa
Copper Cu	130 GPa	129/102 GPa	0,34	49 GPa	135 GPa
Tin Sn	50 GPa	40 GPa	0,36	18 GPa	60 GPa
Lead Pb	16 GPa	18 GPa	0,44	5.5 GPa	44 GPa

Table 1. Elastic properties of relevant metals

Another analytical approach that leads to upper and lower bounds for the elastic parameters was presented in [4] by HASHIN and SHTRIKMAN. Variational principles in the linear theory of elasticity have been applied to obtain bounds for the effective elastic moduli of arbitrary phase geometry. The resulting formulae for upper and lower bounds of binary structures following this method read:

$$k_1 + \frac{c_2}{\frac{1}{k_2 - k_1} + \frac{3c_1}{3k_1 + 4\mu_1}} \leq k \leq k_2 + \frac{c_1}{\frac{1}{k_1 - k_2} + \frac{3c_2}{3k_2 + 4\mu_2}}, \quad (3)$$

$$\mu_1 + \frac{c_2}{\frac{1}{\mu_2 - \mu_1} + \frac{6(k_1 + 2\mu_1)c_1}{5\mu_1(3k_1 + 4\mu_1)}} \leq \mu \leq \mu_2 + \frac{c_1}{\frac{1}{\mu_1 - \mu_2} + \frac{6(k_2 + 2\mu_2)c_2}{5\mu_2(3k_2 + 4\mu_2)}}.$$

The results for both VOIGT-REUSS and HASHIN-SHTRIKMAN bounds are presented in Table 2. Note that the number in the first column shows the composition of the solder and therefore mass concentrations n have to be converted into volume fractions, c , depending on the mass density ρ of the two components as follows:

$$c_1 = \frac{1}{\left(\frac{n_2 \rho_1}{n_1 \rho_2} + 1 \right)}. \quad (4)$$

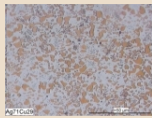
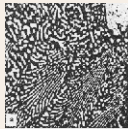
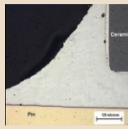
Solder alloy	Microstructure	VOIGT-REUSS bounds	HASHIN-SHTRIKMAN bounds
Ag71/Cu29		$114,4 < k_{\text{hom}}[\text{GPa}] < 115,8$ $34,5 < \mu_{\text{hom}}[\text{GPa}] < 36,2$	$114,7 < k_{\text{hom}}[\text{GPa}] < 114,8$ $34,2 < \mu_{\text{hom}}[\text{GPa}] < 35,4$
Sn62/Pb38		$54,3 < k_{\text{hom}}[\text{GPa}] < 55,2$ $11,1 < \mu_{\text{hom}}[\text{GPa}] < 14,7$	$54,4 < k_{\text{hom}}[\text{GPa}] < 54,6$ $12,7 < \mu_{\text{hom}}[\text{GPa}] < 13,6$
Sn96,5/Ag3,5		$60,18 < k_{\text{hom}}[\text{GPa}] < 60,68$ $18,56 < \mu_{\text{hom}}[\text{GPa}] < 18,68$	$60,27 < k_{\text{hom}}[\text{GPa}] < 60,32$ $18,61 < \mu_{\text{hom}}[\text{GPa}] < 18,62$

Table 2. Results for upper and lower bounds of elastic properties

Obviously the results of both homogenization techniques do not differ significantly. Moreover, the bounds are very close together. Therefore we conclude that not taking the distribution of the specimens in the microstructure

into account is very simplistic and a more sophisticated technique should be considered that acknowledges the internal geometry of the microstructure as well.

A first approach of this kind is given by using a laminate formulae for a SnPb-structure. This seems particularly suitable for coarsened SnPb solders which show lamella-type of structures, such as the ones shown in Figure 5. These develop after a certain time due to the different crystallographic symmetries of tin and lead. In [5] the following equation for YOUNG's modulus in the direction of the lamellae is presented. The index l denotes the properties of the lamella and the index m denotes the properties of the matrix. ν denotes the corresponding Poisson's ratios:

$$E_{11} = c_l E_l + c_m E_m + \frac{4c_l c_m (\nu_l - \nu_m)^2 \mu_m}{[c_m \mu_m / (k_l + \mu_l / 3)] + [c_f \mu_f / (k_m + \mu_m / 3)] + 1}. \quad (5)$$

By using the values given above we obtain $E_{11} = 40.4$ GPa.

In order to compare this result with the homogenized properties determined before, we have to calculate YOUNG's-modulus from the VOIGT-REUSS-bounds of SnPb in Table 2. Since the difference between the POISSON's ratios of both specimens is not that large, we simply conduct a volumetric averaging and obtain $\nu_{\text{SnPb}} = 0.39$. Now by using the relation between YOUNG's modulus and the shear-modulus (average value $\mu = 12.9$ GPa):

$$E = 2\mu(1 + \nu) \quad (6)$$

we find the a homogenized YOUNG's modulus of $E = 35.9$ GPa for SnPb, without taking geometric effects into account. Note that by accounting for the geometric effects of a lamellar structure, YOUNG's modulus has increased by roughly 15%.

3 Effective Elastic Moduli of Heterogeneous Materials

In the previous section formulae for simple geometries or even without geometrical effects have been used. Now an approach will be presented, which is suitable for a general treatment. We consider a loading range so that an elastic response can be assumed. Consequently, HOOKE's law holds:

$$\boldsymbol{\sigma} = \mathbf{C}(\mathbf{x}) : \boldsymbol{\varepsilon}, \quad (7)$$

where $\boldsymbol{\sigma}$ and $\boldsymbol{\varepsilon}$ denote the stress and strain tensors, respectively. $\mathbf{C}(\mathbf{x})$ is the forth-order elastic moduli tensor, which depends on the local position, \mathbf{x} , due to the heterogeneity of the material.

The effective elastic moduli, \mathbf{C}^{eff} , relate the mean (average) stresses and strains through the following relation, which can be found in various publications [6,7,10]:

$$\langle \boldsymbol{\sigma} \rangle = \mathbf{C}^{\text{eff}} : \langle \boldsymbol{\varepsilon} \rangle \quad (8)$$

where:

$$\langle \boldsymbol{\sigma} \rangle = \frac{1}{V} \int_V \boldsymbol{\sigma}(\mathbf{x}) dV, \quad \langle \boldsymbol{\varepsilon} \rangle = \frac{1}{V} \int_V \boldsymbol{\varepsilon}(\mathbf{x}) dV \quad (9)$$

are the mean stresses and strains, averaged w.r.t. a Representative Volume Element (RVE). Obviously mean values should be independent of the chosen domain V provided V is greater or equal than the defined RVE, and so are effective elastic moduli.

By L and l we denote the typical size of the composite material and of the RVE, respectively. The latter contains various material inclusions of size δ (Figure 3). In the case of an alloy the RVE consist of several phases. The

defined sizes are assumed to be related by the inequality $\delta < l \ll L$. Keeping this in mind we introduce a small-scale parameter, ε , by the equation:

$$\varepsilon = \frac{l}{L}. \quad (10)$$

The composite and the RVE are shown in Figure 3. The Cartesian coordinate system (x_1, x_2, x_3) is referred to as the global coordinate system because it describes the whole body. It is useful to introduce a local coordinate system (ξ_1, ξ_2, ξ_3) related to the RVE. ξ_i and x_i , also known as fast and slow coordinates, are transformed via the small-scale parameter ε . Due to that transformation, ξ_i are also Cartesian coordinates. However, they change by the factor $1/\varepsilon$ times faster than the coordinates x_i :

$$\xi_i = \frac{x_i}{\varepsilon}. \quad (11)$$

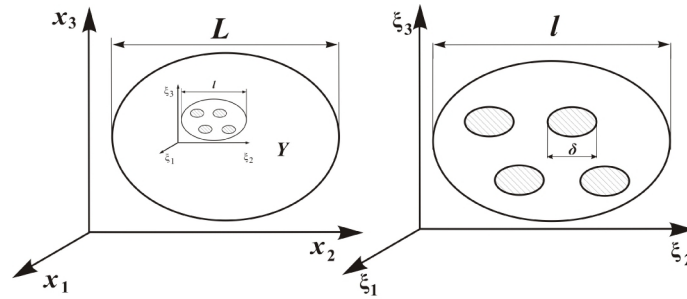


Figure 3. Definition of the Representative Volume Element (RVE)

For a typical Sn-Pb alloy l is about 1.5 microns and $L \sim 0.5$ cm, *i.e.*, 5000 microns (*cf.*, [1,8]). Hence the resulting factor $\varepsilon = 0.0003$ is very small, indeed. The material properties of the heterogeneous structure actually depend on the coordinates ξ_i rather than on x_i , since the heterogeneity of the material is completely represented in the RVE: $C_{ijkl} = C_{ijkl}(\xi_1, \xi_2, \xi_3)$. The global position x_i does not have any impact on material properties. This type of argument can be interpreted as an enlarged point-of-view of the heterogeneous structure.

Now we turn to the most important question how effective moduli can be calculated. The most general solution is considered below [5]. We pose the following boundary-value problem:

$$\begin{cases} (C_{ijkl}(x)u_{k,l})_j = 0 \\ u_i|_{\Sigma} = u_i^0 \end{cases}, \quad i, j, k, l = 1, 2, 3, \quad (12)$$

with displacement boundary conditions $u_i^0 = \varepsilon_{ij}^0 x_j$, where ε_{ij}^0 are constant and do not depend on the coordinates.

Note that a comma denotes partial derivatives with respect to the coordinates x_i . The problem (12) may be formulated in the domain of a RVE or in any domain greater than a RVE. For example, it may be formulated for the whole composite material. This explains why traditionally problem (12) is formulated by using global coordinates, x_i , while it seems more reasonable to formulate it for the RVE by employing a local scale and by using local coordinates, ξ_i .

The procedure of how to determine the effective moduli is as follows. First, we have to solve problem (12) and then calculate the mean stress and strain values. Finally, the effective moduli are calculated by using Equation (8). In fact, this procedure can be simplified slightly because we do not need to calculate the mean strain tensor.

As a matter of fact, the relation $\langle \varepsilon \rangle = \varepsilon^0$ is proved in [5]. The inverse tensor $\mathbf{J}^{\text{eff}} = (\mathbf{C}^{\text{eff}})^{-1}$ can be calculated by means of a similar procedure. For that purpose the boundary-value problem has to be formulated and solved as follows:

$$\begin{cases} (C_{ijkl}(x)u_{k,l})_j = 0 \\ C_{ijkl}u_{k,l}n_j|_{\Sigma} = S_i, \end{cases} \quad (13)$$

where $S_i = \sigma_{ij}^0 n_j$ and σ_{ij}^0 denotes constant stresses. Next the mean strains $\langle \varepsilon_{ij} \rangle$ have to be calculated and, finally, effective compliances J^{eff} are determined by using the following equation:

$$\langle \varepsilon_{ij} \rangle = J_{ijkl}^{\text{eff}} \langle \sigma_{kl} \rangle. \quad (14)$$

It is relatively easy to prove that $\langle \sigma \rangle = \sigma^0$ (see [5] for details). It seems reasonable to define the tensor C^{eff} of Equation (8) as the inverse to J^{eff} defined by the previous equation.

Of course, these procedures are usually implemented only approximately. However, this allows deriving closed-form solutions for the effective moduli. For example, several effective moduli calculation methods employ the ESHELBY solution [5] and allow deriving formulae for composites reinforced by inclusions or by fibers. Note that such formulae provide high accuracy only for small volume fractions of inclusions. Another approach is based on a numerical solution to the boundary-value problem (12). Certainly, a numerical solution is approximate by its very nature. However, its accuracy does almost not depend on the volume fractions of the inclusions or fibers. Laminates seem to be the only example of a composite medium for which exact closed-form formulae have been derived. They are described in the next section within the framework of the so-called multi-scale method.

4 Multi-Scale Method

Some composite materials show a periodic structure. Such a material is composed of a repetitive element which is called periodicity cell. As a matter of fact a periodic cell is the RVE itself. Periodic structures lead to significant simplifications of the solution of problem (12) because it has to be solved only in a domain of one periodicity cell [9]. This is described below with the help of a multi-scale method which utilizes the idea of two scales [6,7]. Indeed, composite materials with periodic structures can be investigated by using at least two scales. The global scale is related to the whole piece of the material. Hence global coordinates, x_i , are used to identify material points. The local scale is related to the periodicity cell only. Consequently, ‘fast’ coordinates, ξ_i , are employed at this level in order to account for the microstructure. A two-scale method effectively utilizes two different scales and represents a solution depending on both ‘slow’ and ‘fast’ coordinates to the global boundary value problem by combination of functions, e.g., a slow-varying global displacement field superposed with a fast-varying local displacement field. Indeed, elastic moduli depend on the periodicity of the cell structure, *i.e.*, on ‘fast’ coordinates only so that $C_{ijkl} = C_{ijkl}(\xi_1, \xi_2, \xi_3)$. Often moduli $C_{ijkl}(\xi)$ are treated as discontinuous piece-wise constant functions of the coordinates ξ . On the other hand, the right-hand side in the equilibrium equation depends usually on ‘slow’ coordinates. Therefore the solution to a boundary-value problem depends on both coordinates as indicated by the following formula:

$$u_i = u_i^{(0)}(\mathbf{x}, \xi) + \varepsilon u_i^{(1)}(\mathbf{x}, \xi) + \varepsilon^2 u_i^{(2)}(\mathbf{x}, \xi) + \dots \quad (15)$$

The multi-scale method is based on the idea of representing the solution of the elasticity problem as an asymptotic series [7]. Equation (15) states that the displacement is represented by an asymptotic series with respect to small parameter ε : the higher the number of periodicity cells, the smaller the parameter ε .

After some modifications, see [6] for Details, the series is simplified to the form:

$$u_i(\mathbf{x}, \xi) = v_i(\mathbf{x}) + \varepsilon N_{ijk}(\xi) v_{j,k}(\mathbf{x}) + \dots \quad (16)$$

where $v(\mathbf{x})$ is the slow-varying displacement part while $N_{ijk}(\xi)$ represents the fast-varying displacement fluctuations. According to the asymptotic nature of the series the first two terms are already sufficient to get a good accuracy for the displacement with a small ε .

Multi-scale methods were developed for solutions of differential equations with fast-varying coefficients, such as the equilibrium equation of linear elasticity:

$$\left(C_{ijkl}(\xi) u_{k,l} \right)_{,j} + f_i(\mathbf{x}) = 0. \quad (17)$$

In particular multi-scale method is used to determine the effective elastic moduli for a periodic medium. With this purpose in mind we substitute the displacement (15) in (13) and collect terms for every power of small parameter ε . The major term has the factor ε^{-1} and must be equal to zero because mathematically speaking ε tends to zero. These results lead to the following relation, which is usually referred to as the cell problem [6,7]:

$$\frac{\partial}{\partial \xi_i} \left(C_{ijkl}(\xi) \frac{\partial N_{ipq}(\xi)}{\partial \xi_i} + C_{ijpq}(\xi) \right) = 0, \quad p, q = 1, 2, 3. \quad (18)$$

This allows us to determine the local displacement functions $N_{ipq}(\xi)$. These functions represent displacements inside the periodic cell. Hence the first subscript denotes the direction of the displacement. The last two subscripts are free and remind us that six local problems have to be solved in the most general case.

The equilibrium relation (17) is supplemented by boundary conditions and a condition $\langle N_{ipq}(\xi) \rangle = 0$. The latter equality simply means that $\mathbf{v}(\mathbf{x})$ is equal to the mean value of displacement $u_i(\mathbf{x}, \xi)$ according to Equation (16). Very often the periodicity cell is a square so that the boundary conditions are periodicity conditions in the sense that the functions N_{ipq} and their derivatives are the same on the left and right hand side faces of the periodicity cell. Certainly the same is true about the top and the bottom, front, and back faces, respectively.

The second outcome from the substitution of (15) into the equilibrium equation is the homogenized equilibrium equation with effective moduli C_{ijpq}^{eff} as coefficients:

$$\left(C_{ijkl}^{\text{eff}} u_{k,l} \right)_{,j} + f_i(\mathbf{x}) = 0. \quad (19)$$

This equation is the result of averaging over the periodicity cell of all terms that are multiplied by ε^0 in the equilibrium equation after substituting the displacements following (15). Strains and stresses are determined by means of the following formulae:

$$\varepsilon_{ij} = \frac{1}{2}(v_{i,j} + v_{j,i}) + \frac{1}{2} \left(\frac{\partial N_{ipq}}{\partial \xi_j} + \frac{\partial N_{jpq}}{\partial \xi_i} \right) v_{p,q}, \quad \sigma_{ij} = C_{ijkl}(\xi) \frac{\partial N_{kpq}(\xi)}{\partial \xi_l} + C_{ijpq}(\xi) \quad (20)$$

which are derived by direct differentiation of the displacements (15).

Now it is easy to understand why the multi-scale method presents a way to calculate effective moduli as additional outcome. In fact, if it is used to solve the boundary-value problem (12), some simplifications will arise. In such a case, the linear displacements $v_i = \varepsilon_{ij}^0 x_j$ give an exact solution to the homogenized equilibrium equation and satisfy the boundary conditions in the boundary-value problem (12). Therefore, stresses and strains in problem (12) are given by (20).

Then, their mean values are as given by $\langle \sigma_{ij} \rangle = \left\langle C_{ijkl}(\xi) \frac{\partial N_{kpq}(\xi)}{\partial \xi_l} + C_{ijpq}(\xi) \right\rangle \varepsilon_{pq}^0$, $\langle \varepsilon_{ij} \rangle = \varepsilon_{pq}^0$ and, effective elasticity moduli have the following form:

$$C_{ijpq}^{\text{eff}} = \left\langle C_{ijkl}(\xi) \frac{\partial N_{kpq}(\xi)}{\partial \xi_l} + C_{ijpq}(\xi) \right\rangle. \quad (21)$$

Now we consider a laminated composite material as shown schematically in Figure 4a. We choose $x_3(\xi_3)$ to be situated across the direction of the layers. The periodicity cell is composed of several layers of different materials. In this case the local equation (18) appears to be an ordinary differential equation. Its solution followed by averaging results in an exact closed-form formula for effective moduli:

$$C_{ijnk}^{\text{eff}} = \langle C_{ijnk} \rangle + \langle C_{ijm3} C_{m3i3}^{-1} \rangle \langle C_{i3p3}^{-1} \rangle^{-1} \langle C_{p3q3}^{-1} C_{q3nk} \rangle - \langle C_{ijm3} C_{m3i3}^{-1} C_{i3nk} \rangle. \quad (22)$$

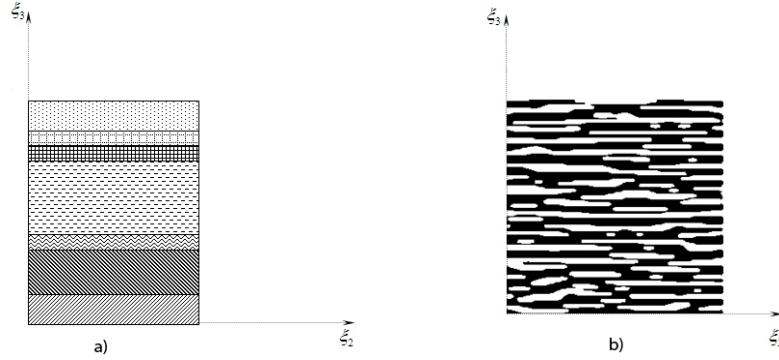


Figure 4. a) Model layered structure; b) Tin-lead solder structure

In Figure 4b we can see a Sn-Pb solder structure composed of tin and lead layers. In the next section we use two approaches for calculating its effective moduli. First, we use the finite element method to solve (12) in the RVE directly. Second, we use Equation (22) because the solder structure is very similar to a layered structure as can be seen in Figure 4b. In the case of plane elasticity the formulae simplify to become:

$$\begin{aligned} C_{2222}^{\text{eff}} &= \langle C_{2222} \rangle + \langle C_{3333}^{-1} \rangle^{-1} \langle C_{2233} C_{3333}^{-1} \rangle^2 - \langle C_{2233}^2 C_{3333}^{-1} \rangle, \\ C_{3333}^{\text{eff}} &= \langle C_{3333}^{-1} \rangle^{-1}, \\ C_{2233}^{\text{eff}} &= \langle C_{3333}^{-1} \rangle^{-1} \langle C_{2233} C_{3333}^{-1} \rangle, \\ C_{2323}^{\text{eff}} &= \langle C_{2323}^{-1} \rangle^{-1}. \end{aligned} \quad (23)$$

By taking into account that the solder under consideration is composed of two phases with volume fractions v_1 and v_2 , respectively, we get:

$$\begin{aligned} C_{2222}^{\text{eff}} &= v_1 \cdot C_{2222}^{(1)} + v_2 \cdot C_{2222}^{(2)} + \\ &\quad \left[C_{2233}^{(1)} \frac{v_1}{C_{3333}^{(1)}} + C_{2233}^{(2)} \frac{v_2}{C_{3333}^{(2)}} \right]^2 \cdot \frac{C_{3333}^{(1)} C_{3333}^{(2)}}{v_1 \cdot C_{3333}^{(2)} + v_2 \cdot C_{3333}^{(1)}} - \left[C_{2233}^{(1)} \right]^2 \cdot \frac{v_1}{C_{3333}^{(1)}} - \left[C_{2233}^{(2)} \right]^2 \cdot \frac{v_2}{C_{3333}^{(2)}}, \\ C_{3333}^{\text{eff}} &= \frac{C_{3333}^{(1)} \cdot C_{3333}^{(2)}}{v_1 \cdot C_{3333}^{(2)} + v_2 \cdot C_{3333}^{(1)}}, \\ C_{2323}^{\text{eff}} &= \frac{C_{2323}^{(1)} \cdot C_{2323}^{(2)}}{v_1 \cdot C_{2323}^{(2)} + v_2 \cdot C_{2323}^{(1)}}, \\ C_{2233}^{\text{eff}} &= \left(v_1 \cdot \frac{C_{2233}^{(1)}}{C_{3333}^{(1)}} + v_2 \cdot \frac{C_{2233}^{(2)}}{C_{3333}^{(2)}} \right) \cdot \frac{C_{3333}^{(1)} \cdot C_{3333}^{(2)}}{v_1 \cdot C_{3333}^{(2)} + v_2 \cdot C_{3333}^{(1)}}. \end{aligned} \quad (24)$$

5 Effective Elastic Properties of a SnPb-Alloy

Traditionally tin-lead alloys are widely used as microelectronic solders. Micro-structural diffusion occurs during the lifetime of the solder due to various external influences. Consequently, the structure of the alloy changes and this, in turn, leads to changing material properties. In this section we conduct a relatively simple study in order to answer the question of how much the solders effective *moduli of elasticity* change depending on a micro-structural variation. A more advanced study on homogenization of the change of the *plastic* properties of alloys will be presented in a later paper. Then it will be investigated how significantly homogenized yield stresses and tangent moduli depend on micro-structural change. Certainly, the most challenging question concerns the formation of cracks, voids or other type of damage that can result in the solder destruction and the breakdown of the functionality of the component.

For the purpose of finding the effective elastic moduli we consider a tin-lead alloy as a two-phase (or two-component) composite structure as shown in Figure 5. The sequence of pictures in this figure shows the development of the microstructure over time. These micrographs have been generated by solving an extended diffusion equation to predict the local concentrations of the constituents of the solder [8]. In addition to the classical driving force for phase separation introduced by CAHN-HILLIARD, an additional term has been introduced, which accounts for the coupling of the mechanical and the thermodynamical problem. The pictures show the typical lamella-type structure of SnPb solders, which occur due to the tetragonal crystal symmetry of the Sn-specimen. Sampling moments of the pictures in Figure 5 are 0.2, 0.5, 1.0, 2.0, 5.0, 10.0 and 20.0 seconds, respectively. The solder is quenched from 183°C down to the 20°C without mechanical loads: No external stresses, which would have an impact on coarsening rate and the developing microstructure, have been applied. One can see that the phases become larger during diffusion. However, due to mass conservation, the volume ratios of the phases are close to constant with quite good accuracy as shown in Table 3. More information about the coarsening in SnPb solders can be found in [8].

Time (s)	Effective elastic moduli of SnPb (GPa)					
	C_{2222}	C_{2233}	C_{3333}	C_{2323}	Volume fraction	
					Sn	Pb
0.1	68.118	43.13975	57.89635	17.33439	0.418747	0.581253
0.2	68.28854	43.14284	57.97969	17.35716	0.421997	0.578003
0.5	68.42638	43.15011	58.04856	17.3767	0.425079	0.574921
1	68.65148	43.15441	58.15837	17.40665	0.430038	0.569962
2	68.53788	43.15237	58.10065	17.39099	0.427139	0.572861
5	68.79415	43.16218	58.23107	17.42867	0.431854	0.568146
10	68.91313	43.08686	58.20988	17.41485	0.430069	0.569931
20	69.1416	43.01026	58.24527	17.41563	0.430725	0.569275

Table 3. Effective moduli of SnPb at different times

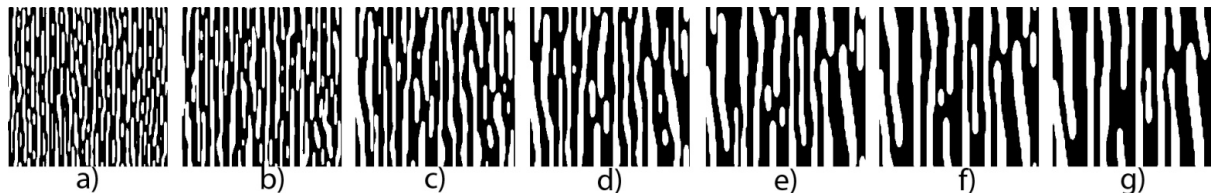


Figure 5. Tin-lead alloy structure change caused by diffusion

We conducted calculations in order to study how much the effective elastic moduli change during the diffusion process. The two methods that we used in order to determine effective moduli of elasticity were explained in the previous section. First, we used a method based on direct numerical solution of the plane elasticity boundary-value problem (12) and formula (8). This formula now reads:

$$\langle \sigma_{ij} \rangle = C_{ijkl}^{\text{eff}} \varepsilon_{kl}^{(0)}, \quad (25)$$

where $\langle \sigma_{ij} \rangle$ are the average stresses of the RVE. It should be emphasized that this approach is just the numerical implementation of the definition of effective moduli as given by Equations (12) and (8). If we put $\varepsilon_{\alpha\beta}^{(0)} = \varepsilon^{(0)} \delta_{\alpha\beta}$, then we get effective moduli $C_{ij\alpha\beta}^{\text{eff}} = \langle \sigma_{ij} \rangle / \varepsilon^{(0)} \delta_{\alpha\beta}$ for $i, j, \alpha, \beta = 2, 3$ from (8). $\delta_{\alpha\beta}$ stands for Kronecker's delta. All subscripts assume the values 2, 3 because plane strain is assumed and the first axis is directed in perpendicular direction.

Second, we determined the effective moduli by using closed-form formulae (24) and kept in mind that the structure of the alloy is similar to a layered composite.

Note that the first method is general whereas the second one is only valid for structures similar to a layered setup. It is important to underline that both methods resulted in almost the same effective moduli values. The main result of the calculations conducted can be formulated as follows: Microstructural change barely affects the outcome of the effective moduli.

For example, Figure 6 gives the time dependence of modulus $C_{2323}(t)$. Every value $C_{2323}(t)$ on the graph corresponds to the moment of time, for which the picture of the microstructure was provided. These pictures were obtained by means of diffusion simulation developed in [8]. The blue diamonds in Fig. 6 represent $C_{2323}(t)$ calculated when using the first method, while brown square points show the variation of C_{2323} in time determined from the closed-form formulae. The points are very close to each other so that the relative difference varies from 0.5% to 2%. Obviously, the closed-form formulae developed for layered material provide a good approximation tool for the effective moduli of the alloy. We also observe that all effective moduli vary very little. As an example the effective modulus C_{2323} will be examined in more depth. Its changes are comparable to the changes in phase volume ratios or to the accuracy of calculations. Table 3 shows the effective moduli calculated at different times of the structure of the alloy shown in Fig. 5.

Two conclusions can be drawn. First, the effective moduli of the alloy depend only on volume fractions of the phases but not on the detailed structure of the alloy. Second, the effective moduli do not change during diffusion.

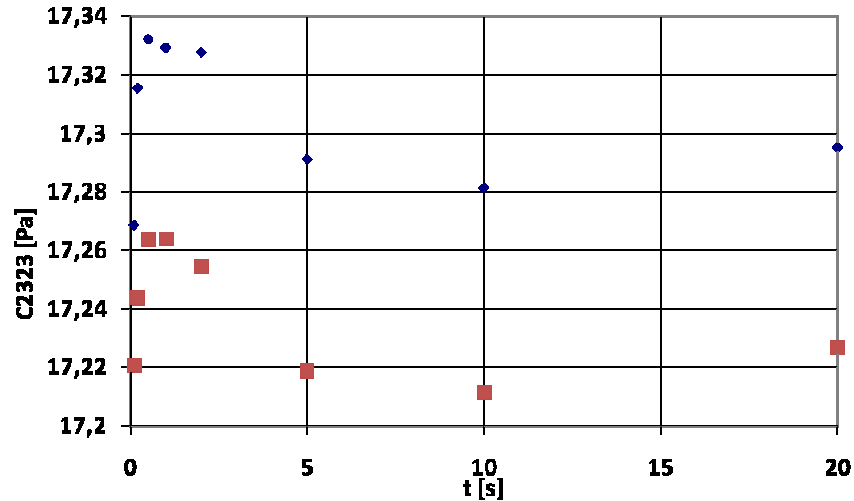


Figure 6. Variation of the effective modulus C_{2323} during diffusion

Fig. 7 shows the relative difference $\frac{\Delta C}{C_{\text{numerical}}}$ in moduli calculated using the two different methods explained above. The difference appears to be smaller towards the end of the diffusion process. However, this result is questionable since the difference is very small and comparable to the accuracy of the calculations and within the “discretization noise” of the picture.

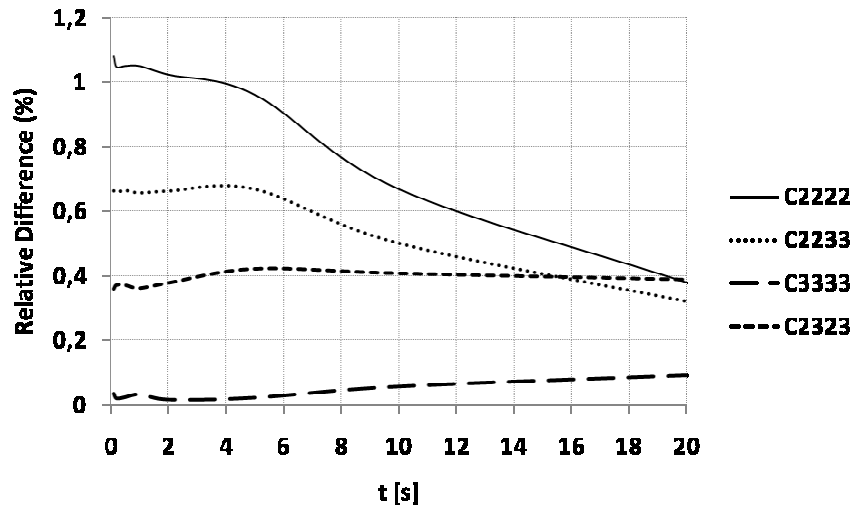


Figure 7. Relative difference between effective moduli

6. Effective Moduli of a Composite with Inclusions

We studied the dependence of the effective moduli on a composite structure containing a varying volume fraction of tin c_{Tin} in the range 0.14 to 0.41 by using the two approaches again. The first method is based on closed-form formulas for fibrous composite taken from [5], while the second one employs direct numerical simulation, i.e., it is numerical solution of the boundary-value problem (12) in the same way as described in previous section. In order to do this a computer program was written, which generates different composite structures. All inclusions are assumed to be circles of different radii. The generated RVEs are shown in Figures 8 - 10.

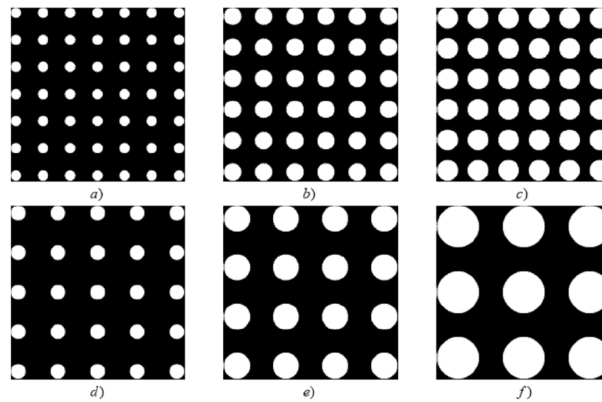


Figure 8. The set of regular structures where inclusions are aligned with nodes of square grid

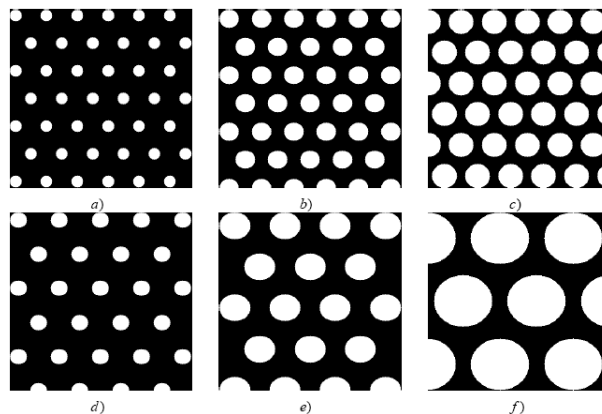


Figure 9. The set of regular structures where inclusions are aligned with nodes of triangular grid

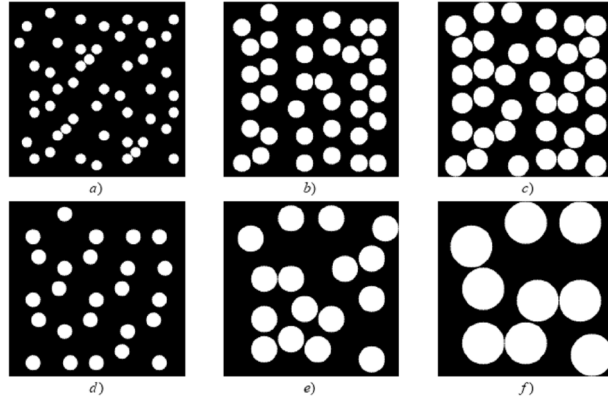


Figure 10. The set of irregular structure

Tin inclusions are shown in the figures as white circles. We considered three types of structures: Two of them are periodical and the third one is irregular. In the case of periodical structures, the centers of the inclusions are aligned along a regular grid. We use grids with square and triangular patterns. In the case of an irregular grid, the grid nodes are distributed according to random deviations from the square grid nodes. The computer program developed allows generating composite structure of these types for given volume fraction of tin and RVE size.

The volume fractions of composite structures shown in Figures 8 – 10 are given in Table 5.

a)	$c_{\text{Tin}} = 0.14$	b)	$c_{\text{Tin}} = 0.28$	c)	$c_{\text{Tin}} = 0.41$
d)	$c_{\text{Tin}} = 0.14$	e)	$c_{\text{Tin}} = 0.28$	f)	$c_{\text{Tin}} = 0.41$

Table 5. Volume fractions of the composite structures in Fig. 8-10

It seems reasonable to give a few more details regarding the first method. The formulae for effective moduli for structures that are shown in Figures 8 - 10 can be easily obtained by using the well-developed theory of unidirectional fiber composites. Indeed, we can assume that the fibrous composite is such that the fibers are directed perpendicular to the planes shown in Figures 8 - 10. With this idea in hand, we apply formulae for the in-plane effective moduli from [5], as an example. The plane that is perpendicular to the fibers is isotropic for a homogenized material in the case of structures with triangular and random inclusions distribution. On the other hand, it is orthotropic for square grid structures. All formulae that we are going to employ were developed for fibrous composites that are transversally-isotropic in macro-scale. This means they can be employed for structures shown in Figures 9 - 10. In the case of a square grid (see Fig. 8) they only provide a way of getting an approximation for the effective moduli and the accuracy that they provide has to be discussed. On the other hand, in contrast to the formulae for the layered medium, which were taken from fibrous composite theory, they are approximate even for triangular and random grid nodes distribution. The accuracy decreases with the growth of volume fraction. Therefore, it seems that the same formulae can be used approximately in the case of square nodes distribution.

In fibrous material theory fibers are usually assumed to be randomly distributed in cross-plane, so it is isotropic in terms of effective homogeneity. Therefore, there are two independent elasticity moduli: the bulk modulus K_{23} and the shear modulus μ_{23} in that plane. Consequently, the relationship of different moduli in the plane of isotropy is as follows [5]:

$$\begin{aligned}
 C_{2222}^{\text{eff}} &= C_{3333}^{\text{eff}} = \mu_{23}^{\text{eff}} + K_{23}^{\text{eff}}, \\
 C_{2233}^{\text{eff}} &= -\mu_{23}^{\text{eff}} + K_{23}^{\text{eff}}, \\
 C_{2323}^{\text{eff}} &= \mu_{23}^{\text{eff}}.
 \end{aligned} \tag{26}$$

Hence the task is to get the closed-form formulae for in-plane bulk and shear moduli. The formula for the effective bulk modulus, K_{23}^{eff} , was derived in [10, 11] and the one for the effective shear modulus, μ_{23}^{eff} , was derived in [12]:

$$K_{23}^{\text{eff}} = k_{\text{Lead}} + \frac{\mu_{\text{Lead}}}{3} + c_{\text{Tin}} \cdot \left(\frac{1}{k_{\text{Tin}} - k_{\text{Lead}} + \frac{1}{3}(\mu_{\text{Tin}} - \mu_{\text{Lead}})} + \frac{1 - c_{\text{Tin}}}{k_{\text{Lead}} + \frac{4}{3}\mu_{\text{Lead}}} \right)^{-1}, \quad (27)$$

$$\mu_{23}^{\text{eff}} = \mu_{\text{Lead}} \cdot \left(1 + c_{\text{Tin}} \cdot \left(\frac{\mu_{\text{Lead}}}{\mu_{\text{Tin}} - \mu_{\text{Lead}}} + \frac{k_{\text{Lead}} + \frac{7}{3}\mu_{\text{Lead}}}{2k_{\text{Lead}} + \frac{8}{3}\mu_{\text{Lead}}} \right)^{-1} \right). \quad (28)$$

It should be pointed out that the formula for μ_{23}^{eff} is correct only for a volume fraction of inclusion that is not greater than 0.2. For greater volume fractions the calculations are slightly more complicated and quadratic equations have to be solved [5].

The approximate nature of the formulae we use is a reason for comparing both approaches and evaluating the accuracy of the closed-form formulas. Effective moduli calculated by using direct numerical calculation are given in Table 6.

VF	N	C_{2222}			C_{2233}			C_{3333}			C_{2323}		
		Sq	Tr	R	Sq	Tr	R	Sq	Tr	R	Sq	Tr	R
0.14	49	109.19	108.83	107.37	57.39	58.03	58.15	109.19	109.2	107.36	25.09	25.36	24.89
	25	110.73	109.19	107.73	57.74	58.15	58.03	110.73	108.98	108.73	25.9	25.25	24.67
	16	110.82	108.97	107.6	57.65	57.87	57.93	110.82	108.67	107.47	26.35	25.41	24.78
	9	112.4	109.58	108.76	57.96	57.92	58.06	112.4	109.3	107.6	27.54	25.83	25.49
	4	116.25	111	107.37	58.83	58.04	57.73	116.25	110.75	108.01	30.29	26.87	24.73
0.28	144	137.86	135.62	135.16	66.55	68.98	68.65	137.86	134.66	138.02	30.19	31.18	31.17
	36	137.56	134.98	134.22	66.76	68.72	67.75	137.56	134.25	134.65	31.54	31.59	30.66
	16	139.17	138.8	134.91	67.16	68.71	68.42	139.17	135	133.7	33.47	32.49	32.23
	9	141.78	137.09	137.25	67.85	68.22	67.91	141.78	136.48	133.54	35.86	34.43	32.08
	4	148.27	138.84	135.16	69.7	68.06	68.52	148.27	136.23	135.2	41.25	34.96	33.55
0.41	144	167.83	164.94	164.77	75.48	79.76	78.11	167.83	161.75	169.56	35.5	37.97	36.99
	36	169.34	169.97	167.09	76.52	80.07	79.96	169.34	162.03	167.85	37.55	39.31	39.33
	16	171.88	173.29	166.57	77.49	80.45	80.15	171.88	163.79	169.3	40.29	40.84	40.28
	9	174.86	176.67	171.89	78.52	80.75	79.42	174.86	165.79	170.97	43.42	42.5	41.39
	4	182.84	183.9	164.89	81.21	81.65	78.52	182.84	169.98	170.54	50.67	46.08	39.76
0.5	64	204.72	202.82	203.68	86.46	92.58	90.41	204.72	198.28	208.41	42.32	47.11	44.73
	25	205.19	205.98	200.95	87.47	93.08	90.75	205.19	201.69	206.59	44.84	48.94	45.66

Table 6. Effective moduli for different distributions of inclusions

In Table 6 VF stands for the Volume Fraction of Sn (tin), Sq means SQUARE grid, Tr and R refer to TRIangular and Random grids, respectively; N is the number of inclusions.

An analysis of the results given in the Table 6 leads to the following conclusions: The first one concerns the RVE size. It could be revealed that the RVE must include at least four inclusions for a regular square grid. For a regular triangular grid and an irregular grid the RVE can be smaller. This is true for any considered volume. Once the ratio is constant the effective moduli change little if the RVE size increases. The relative difference is about 1%. Therefore, we can conclude that the effective moduli within the RVE depend on the volume fractions of the phases only. Moreover, if the volume fraction is constant, the effective moduli do not depend on the grid type, too.

As an example the modulus $C_{2222}(c)$ is shown in Figure 11 as a function of the volume fraction, c , of the inclusions. Again the modulus was determined by using the numerical method based on a solution of the boundary-value problem (11) and by approximate closed-form expressions valid for small fibers volume fractions. The

numerically determined modulus $C_{2222}(c)$ is indicated by a dotted line. The modulus calculated by virtue of closed-form expressions is represented by a solid line.

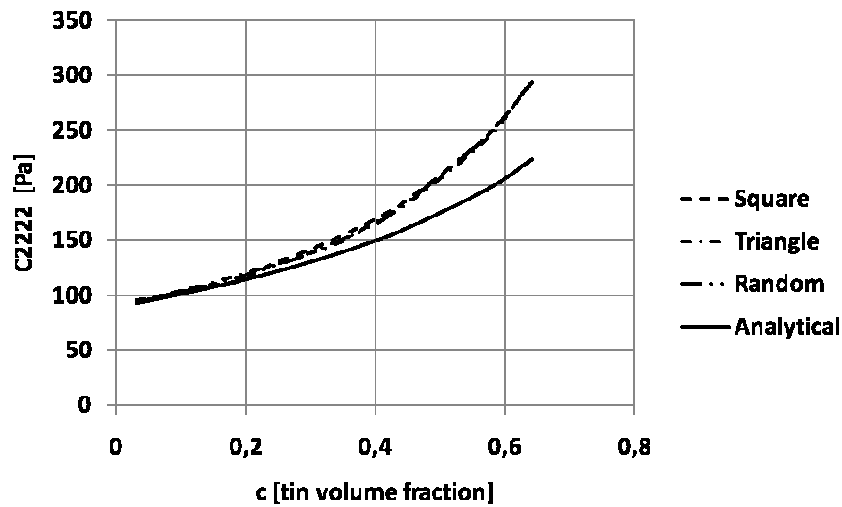


Figure 11. Tin volume fraction dependence of C_{2222}

The graphs for the other effective moduli are qualitatively the same. It is clear that the closed-form solutions provide a good approximation only for volume fractions of the inclusions that are less than 0.2. Within this range the accuracy of the formulae is less than 5%. It should be noted that the accuracy of the formulae (23) for the structure shown in Figure 5 is about 0.5%-2%.

The second remark concerns the effect of different distributions of inclusions. Figure 9 shows that the effective moduli calculated for square, triangle and random grids are very close to each other. This simply means that the effective moduli depend on the volume ratio of the inclusions and that they do not depend on the details of the distribution of the inclusions. The number of the inclusions and their alignment shows no impact on effective moduli.

The calculations described in this section validate once again that the structural change during the diffusion process does not influence the effective moduli of elasticity of a solder.

7 Conclusion and Outlook

As it was shown in Section 2 of this paper, the geometry and therefore the distribution of the constituents in the microstructure has an influence on mechanical properties which cannot be neglected. Moreover the analysis of the results of the multi-scale approach clearly shows that a microstructure changing with time has no influence on the elastic properties. This can be interpreted in the following manner. Since in the presented solder alloys the type of the microstructure (*e.g.*, lamellae, grains of essentially circular shape) does not change during the coarsening process and just the geometric distribution of the structures is different, the elastic parameters are constant over time. Nevertheless, although the development in time can be neglected, the influence of the microstructure on elastic properties is of interest due to formation of certain geometries in the early stages of phase separation. An alloy that develops a lamella-type of microstructure will give different effective elastic moduli than, *e.g.*, an alloy composed of cubic constituents that will form a grain-type microstructure although the concentrations of inclusions might be the same. Note that the presented results just hold for elastic properties. Non-linear material laws for plastic and creep deformations are a topic of current interest. As the presented multi-scale method has been proven to be a powerful tool for that kind of structures, an adaption for non-linear material behavior is required. As solders are frequently subjected to the thermo-mechanical fatigue loading, further examinations are aimed to apply the presented methods to such kind of material behavior.

References

- [1] Müller, W.H., Böhme, T.: Quantitative description of micro-structural changes in lead-free solder alloys. *Electronics Packing Technology Conference*, 390–397, 2006.
- [2] Böhme, T., Dreyer, W., Müller, W.H.: Determination of higher gradient coefficients by means of the Embedded-Atom-Method, *Cont. Mech. Thermodyn.*, 18, 411-441, 2007.
- [3] Nye, J.F.: Physical properties of crystals, *Oxford University Press*, 140-145, 1957.
- [4] Hashin, Z., Shtrikman, S.: A variational approach to the theory of the elastic behaviour of multiphase materials, *J. Mech. Phys. Solids*, 11, 127-140, 1963.
- [5] Christensen, R.M.: Mechanics of composite materials. *J. Wiley*, 2nd ed., 1979.
- [6] Pobedrya, B.E.: Mechanics of composite materials. *Moscow State University Press*, 1984 (in Russian).
- [7] Bakhvalov, N.S., Panacenko, G.P.: Homogenization: Averaging processes in periodic media. Mathematical problems in the mechanics of composite materials, *Kluwer Academic Publishers*, Dordrecht, 1994.
- [8] Dreyer, W., Müller, W.H.: A study of the coarsening in tin/lead solders. *International Journal of Solids and Structures*, 37, 3841-3871, 2000.
- [9] Bardzokas, D.I.: Mathematical modelling of physical processes in composite materials of periodical structures. *URSS Editorial*, 2003.
- [10] Hill, R.: Theory of mechanical properties of fibre-reinforced materials. I. Elastic behaviour. *J. Mech. and Phys. Solids*, 1964, v.2, p. 166.
- [11] Hashin Z. Viscoelastic fiber reinforced materials. *AIAA Journal*, 1966, V.4, p.1411.
- [12] Christensen R.M., Lo K.H. Solutions for effective shear properties in three phase sphere and cylindrical models. *J. Mech. and Phys. Solids*, 1979, v.27, No.4

Addresses:

Dipl.-Ing. Andreas Brandmair, Technische Universität Berlin, Fak. V, Institut für Mechanik, Lehrstuhl für Kontinuumsmechanik und Materialtheorie, MS2, Einsteinufer 5, D-10587 Berlin,
email: andreas.brandmair@tu-berlin.de

Prof. Wolfgang H. Müller, Technische Universität Berlin, Fak. V, Institut für Mechanik, Lehrstuhl für Kontinuumsmechanik und Materialtheorie, MS2, Einsteinufer 5, D-10587 Berlin,
email: wolfgang.h.mueller@tu-berlin.de

Margerita Savenkova, Lomonosov Moscow State University, GSP-2, Leninskie Gory, Moscow, 119992, Russia,
email: madgista@gmail.com

Prof. Sergey Sheshenin, Lomonosov Moscow State University, GSP-2, Leninskie Gory, Moscow, 119992, Russia, email: sergey.sheshenin@mail.ru